ACS OMEGA

Article

Cite This: ACS Omega 2019, 4, 21302−21310

http://pubs.acs.org/journal/acsodf

Molten Salt Hydrates in the Synthesis of TiO_2 Flakes

Trang Q. Tran,[†] Weiqing Zheng,[‡] and George Tsilomelekis*[,†]

[†]Department of Chemical and Biochemical Engineering, Rutgers, The State University of New Jersey, Piscataway, New Jersey 08854, United States

[‡]Catalysis Center for Energy Innovation and Department of Chemical and Biomolecular Engineering, University of Delaware, Newark, Delaware 19716, United States

Supporting Information

ABSTRACT: Herein, we present a method for the preparation of titanium dioxide with a relatively large surface area, mesoporosity, and good thermal stability. We show that by utilizing molten salt hydrates (MSH) as non-trivial synthesis media, we prepare materials with thin, flake-like morphology with a large aspect ratio. The thickness of the synthesized flakes can be controlled by adjusting the salt/water (always in the MSH regime) and/or the salt/precursor molar ratio. The TiO_2 flakes appear to be formed via the aggregation of small TiO_2 nanoparticles (typically around 7−8 nm) in an apparent 2D morphology. We hypothesize that the ordered structure of water molecules within the ions of the salt in conjunction with the fast hydrolysis/condensation rates occurring in the presence of water of the precursor used are responsible for this agglomeration. We also report that the purity of materials (anatase vs brookite crystalline phase) appears to be a function of the LiBr/water ratio which is hypothesized to arise either from pH variation or due to lattice matching of the relevant orthorhombic structures (brookite and $LiBr_x{\cdot}3H_2O$). Discussion on the potential for scalability of the presented method is also highlighted in this article.

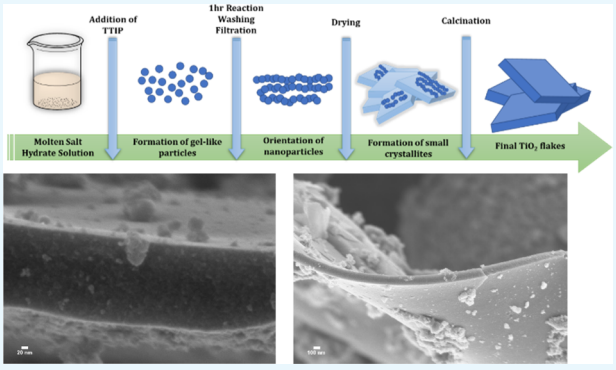

1. INTRODUCTION

The undoubtable importance of titanium dioxide (TiO_2) is underscored by its vast potential applications in various fields encompassing but not limited to sensing,[1−3] lithium-, aluminum-, and sodium-ion batteries,[4−6] dye-sensitized solar cells,[7−10] and catalysis.[11−14] The reasons behind the versatility of TiO_2 lie in its intrinsic properties such as low cost, nontoxicity, chemical stability, acidity, specific surface area, and relatively good thermal stability. These properties of TiO_2 have led to the development of a variety of metal or metal oxide catalysts supported on TiO_2 surfaces that can be utilized in highly important catalytic reactions such as the selective NO_x reduction,[15] hydrodesulfurization,[16] water−gas shift,[17] oxidative dehydrogenation,[18−20] and so forth. Besides thermal catalysis, TiO_2 finds wide applications in photocatalytic reactions due to its very good semiconducting properties.[13,21−23] Among the crystalline phases of TiO_2, anatase has been widely utilized in the field of catalysis primarily due to its higher surface area as compared to the other phases.[24−26] TiO_2 with mixed crystalline phases such as anatase−rutile or anatase−brookite have shown improved chemical stability as well as photocatalytic activity with the former being the most common mixture employed.

Research endeavors have been aimed at controlling the morphology and crystalline structure of TiO_2, which in turn control its physicochemical properties, by applying different synthesis protocols.[24] Various structural designs have been reported including TiO_2 spheres, fibers and tubes, nanosheets, films, and larger interconnected architectures and their relevant properties are discussed elsewhere.[27] TiO_2 in the form of thin flakes, films, nanosheets, or even 2D structures has received considerable attention due to their enhanced reactivity in photocatalytic as well as in several heterogeneous catalytic reactions.[28] The reasons behind the promising catalytic behavior associated with these materials stem from the numerous opportunities that exist to tune the morphology and molecular structure during synthesis and post-treatment. Besides their high specific surface area, the possible exposure of the [001] high-energy facet has been predominantly underscored in the open literature as among one of the reasons behind the improved reactivity of TiO_2 sheets.[29,30] In the anatase crystalline form of titanium dioxide, the [001] is present as a small fraction because the [101] usually dominates the nanocrystalline particles. The recent interest in facet-controlled design of TiO_2 has led research endeavors to be focused on developing synthetic protocols where nanoparticles with high portion of exposed [001] facet are organized to form 2D-like TiO_2 materials.[30] These materials have an apparent 2D morphology because they present a thickness of few nanometers as opposed to 2D nanosheets derived usually via

Received: September 3, 2019
Accepted: November 18, 2019
Published: December 3, 2019

DOI: 10.1021/acsomega.9b02850
ACS Omega 2019, 4, 21302−21310

Scheme 1. Schematic Representation of the Sequence of the Proposed Steps to Prepare TiO_2 Flakes

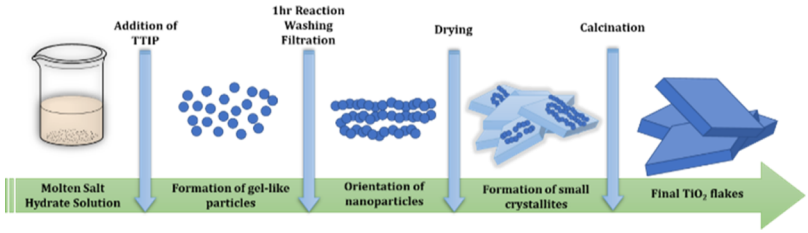

exfoliation of titanates that present thickness at the molecular or even atomic level.[31] This field has experienced rapid growth recently due to the potential applications in Li-ion batteries as anodes and in dye-sensitized solar cells; several authors have reported novel approaches that utilize surface capping agents to control exposed facets which in turn can guide chemical reactivity. However, scaling up these synthetic protocols is hampered by the fact that the highly toxic hydrofluoric acid is usually employed in high concentrations.

Molten salt synthesis (MSS) has been reported as an efficient method to synthesize a vast number of metal oxides by utilizing a melting salt as a solvent. The MSS method is a nonaqueous route that allows the synthesis of relatively thermally and chemically stable metal oxides; as water is absent, highly reactive metal oxide precursors have been also used.[32] Recently, the MSS method has been reported to produce TiO_2 nanosheets that exhibit improved capacity as compared to the bare TiO_2, as well as better activity in dye-sensitized solar cells.[33,34] The free ions in the molten salt medium have been underscored to be instrumental in binding the high-energy facets and consequently stabilizing them. In general, the MSS method is simple and versatile and recently has been highlighted as being scalable for the production of 2D oxides and hydroxides due to its short reaction time (~1 min).[35] Although through the MSS route, highly crystalline materials with controlled facets can be synthesized,[36] the high operating temperature comprises the main drawback considering potential industrial realization.

Besides the effect of the free ions in the molten salt route, very recently, the nature of salt solid crystals has been underscored to play a key role in a novel synthetic approach.[37] In this synthetic strategy, metal oxide precursors were first dissolved in ethanol to avoid rapid nucleation of oxide nanocrystals and then a small amount of the solution was mixed with a large amount of solid salt crystals. It is hypothesized that the lattice matching between the salt solid crystals and the desired growing metal oxide is pivotal in controlling the 2D morphology, whereas the salt/precursor ratio controls the thickness of the final oxide. The excess ethanol used in conjunction with the large amount of solid salt crystals (making the synthesis medium highly heterogeneous) could be considered as the main drawbacks of this method.

In this work, we report a novel and simple synthesis strategy where molten salt hydrates (MSH) are utilized as solvents for the production of TiO_2 flakes. We hypothesize that the ordered structure of the MSH medium is responsible for guiding the agglomeration of small TiO_2 nanoparticles (~7−8 nm) to an apparent 2D-like morphology with a large aspect ratio and tunable thickness. Specifically, aqueous lithium bromide (LiBr) solutions with various H_2O/salt molar ratio, always within the MSH regime, have been investigated in order to study possible morphological and structural changes of TiO_2. This new synthesis strategy occurs at nearly ambient temperature and short reaction times due to the high reactivity between the TiO_2 precursor and water; calcination comprises the only post-synthesis heat treatment. We also evaluate the effect of salt/precursor as well as water/precursor on controlling the aspect ratio and thickness of the TiO_2 prepared. We use in situ Raman measurements to follow the calcination steps and to evaluate the long-term thermal stability of the prepared materials.

2. EXPERIMENTAL SECTION

2.1. Materials. Titanium(IV) isopropoxide, (99.99% trace metals basis), lithium bromide (ReagentPlus, ≥99%), and titanium(IV) oxide (brookite and rutile) were purchased from Sigma-Aldrich and used without further purification. Titanium-(IV) oxide (anatase) was purchased from Alfa Aesar.

2.2. Synthesis Protocol. Herein, we describe the sequence of all required steps that have been followed in order to prepare the TiO_2 thin flakes. A schematic representation of the synthesis procedure is depicted in Scheme 1.

The first step encompasses the preparation of the solvent medium that is used to conduct hydrolysis and condensation of the precursor. We use MSHs as the reaction medium, that is, solutions with water to salt molar ratio equal to or less than the coordination number of the cation.[38] In a typical synthesis procedure, precalculated amount of lithium bromide (LiBr) is added in 10−15 mL of deionized water in order to prepare solutions in the range of 3.25−5 H_2O/LiBr molar ratio. This range ensures that the solution pertains to the MSH state.[38,39] The prepared solution is maintained at the temperature of 35 °C in an oil bath under stirring for around 30 min. After we ensure that the solution temperature is stable, a known amount (1−5 mL depending on the required scale) of the titanium oxide precursor (titanium isopropoxide, TTIP) is added to the solution under vigorous stirring. After the addition of TTIP, the solution is maintained at 35 °C for 1 h in the presence of reflux in order to promote hydrolysis and condensation of the precursor and form the corresponding titanium hydroxide. Depending on the synthesis conditions, the LiBr/TTIP ratio is controlled in the range of 13−80. The precipitate is filtered with a Büchner funnel under reduced pressure and washed thoroughly with water. In the cases of large LiBr/TTIP, the material can be also recovered by means of centrifugation. The final solid material is collected and dried overnight at 110 °C under static air. The dried whitish powder is calcined at the temperature of 400 °C for 3 h with a ramp of 2 °C/min in a tubular furnace. The calcined material is then used for further characterization.

2.3. Characterization of Materials. Raman spectra were recorded using a HORIBA LabRAM HR Evolution high spatial and spectral resolution spectrometer. The incident beam (532 nm, 80 mW) was directed into a reaction cell (Harrick

DOI: 10.1021/acsomega.9b02850
ACS Omega 2019, 4, 21302−21310

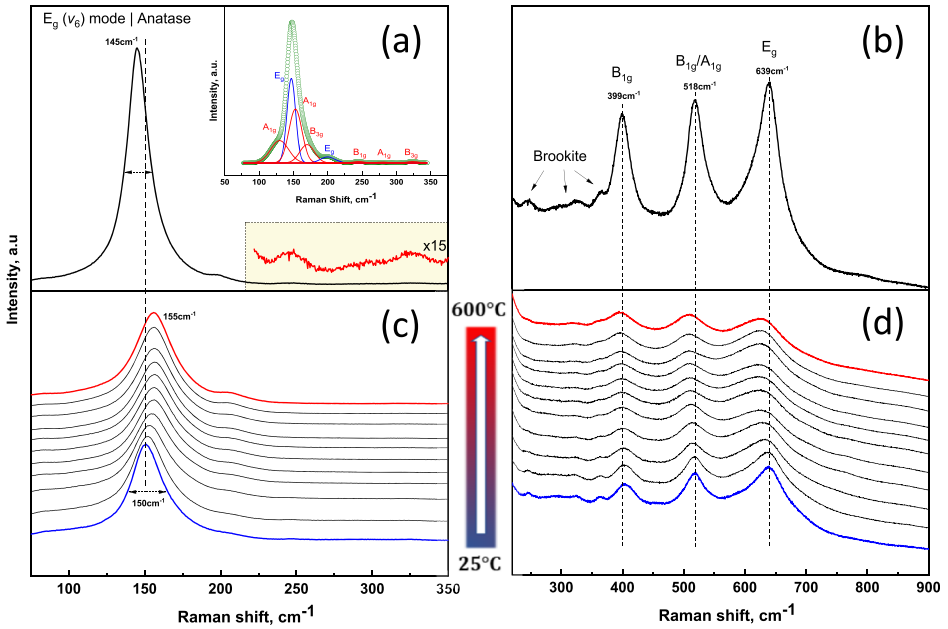

Figure 1. Raman spectrum of TiO_2 prepared after calcination at 400 °C at the (a) 75−350 and (b) 225−900 cm^{-1} spectral ranges. Pertinent deconvolution using Gaussian peaks is depicted as the inset. (c,d) show the in situ Raman calcination data at the same spectral envelopes. The temperature ramp was set to 2 °C/min; spectral collection microscope objective was 100×; laser wavelength was 532 nm.

Scientific Products Inc.) and focused on the sample with a 10× long-working distance objective. Collection of the scattered light was achieved with an air-cooled (−75 °C) open electrode 1024 × 256 pixels CCD. The acquisition time of each spectrum was 20−60 s, the number of accumulations varied in the range of 6−12, and the spectral slit was fixed at 100 μm. A 25−50% neutral density filter was also used to avoid local overheating of the catalyst sample which can cause changes in the measured spectra. For the in situ Raman calcination measurements, air flow is maintained at 50−100 cm^2/min via a mass flow controller (Alicat Scientific).

Scanning electron microscopy (SEM) images were acquired with a Zeiss, Zeiss Sigma field emission scanning electron microscope. Transmission electron microscopy (TEM) images were acquired with a JEM-2010F (JEOL, Japan) transmission electron microscope equipped with a field emission gun emitter. The specific surface area of the prepared TiO_2 samples was estimated through the Brunauer−Emmett−Teller (BET) method using a Quantachrome, Autosorb-1 instrument. The BET measurements were carried out at liquid nitrogen temperature after degassing samples at 150 °C for 3 h.

3. RESULTS AND DISCUSSION

3.1. Thermal Stability and Structural Implications via in Situ Raman Calcination. Figure 1a,b shows the room-temperature Raman spectrum (at two different Raman shift regimes) of the TiO_2 sample that has been calcined at 400 °C and prepared at H_2O/LiBr and LiBr/TTIP equal to 3.25 and 13, respectively. According to the factor group analysis of anatase-TiO_2, six allowed Raman modes can be observed based on the $A_{1g} + 2B_{1g} + 3E_g$ representation. The main band shown in Figure 1a and located at 145 cm^{-1} corresponds to the $E_g(\nu_6)$ vibrational mode of the anatase crystal form of TiO_2. The position as well as the sharp character of this band is indicative of relatively crystalline material. The 198, 399, 518, and 639 cm^{-1} bands correspond to the rest of the optical phonon modes of anatase TiO_2, that is, $E_g(\nu_5)$, $B_{1g}(\nu_4)$, $B_{1g}(\nu_2)$/$A_{1g}(\nu_3)$, and $E_g(\nu_1)$, respectively.[40] A closer look at the 145 cm^{-1} band reveals a slightly asymmetric character toward higher Raman shift, whereas at the 200−350 cm^{-1} spectral regime, multiple low-intensity bands were also observed. The position of these vibrational bands indicates the presence of a brookite crystal in the structure of the synthesized TiO_2. The low intensities of the brookite phase underscore its small fraction in the synthesized material. This observation is in agreement with our X-ray diffraction (XRD) results shown in the Supporting Information (Figure S1), as well as TEM measurements that are discussed later. However, it is worth mentioning that the Raman cross section of each crystalline phase in principle can differ, thus contributing to a different extent in the apparent spectral intensities. According to the Raman spectrum of pure brookite (shown in the Supporting Information as well, Figure S2) high-intensity bands are expected to overlap with the 145 cm^{-1} band and thus a deconvolution of the pertinent spectral envelope is also shown as an inset in Figure 1a.

In an effort to follow the structural changes occurring in our samples upon calcination as well as their intrinsic thermal stability, in situ Raman temperature-dependent spectra have been collected in the 25−600 °C range and are shown in Figure 1c,d. Starting from the dried sample right after the synthesis and prior to any calcination procedure, we collect in situ Raman spectra upon heating with a temperature ramp of 2 °C/min that mimics the calcination process we follow in the tubular furnace, as discussed in the experimental part. All spectra have been normalized and vertically translated for better representation. The spectral envelope of Figure 1c (75−350 cm^{-1}) shows mainly the $E_g(\nu_6)$ vibrational mode of anatase TiO_2, whereas the $E_g(\nu_5)$ appears as a weak shoulder at ∼200 cm^{-1}. It is evident that at 25 °C, our synthesis method leads to TiO_2 material that shows some extent of crystallinity even prior to calcination as underscored by the clear presence of all vibrational modes of anatase (Figure 1c,d). It is worth mentioning here that the $E_g(\nu_6)$ band appears at 150 cm^{-1} as

DOI: 10.1021/acsomega.9b02850
ACS Omega 2019, 4, 21302−21310

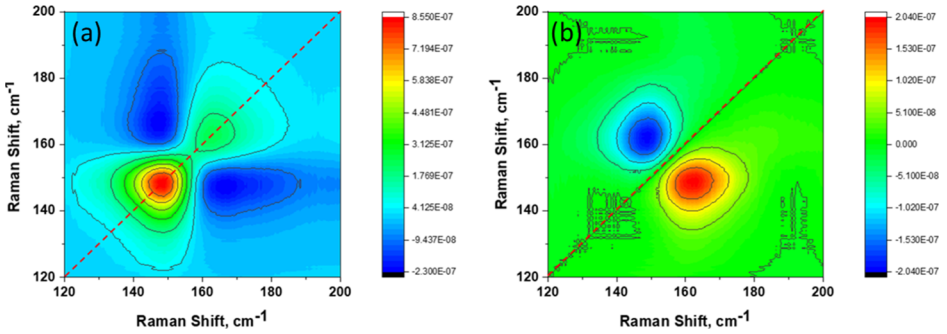

Figure 2. (a) Synchronous and (b) asynchronous 2D Raman maps of titanium dioxide synthesized as a function of temperature. The temperature range used for the generation of the 2D Raman maps was 25−600 °C. The correlation spectra were developed by utilizing the 2D application available in the Origin 2019b software.

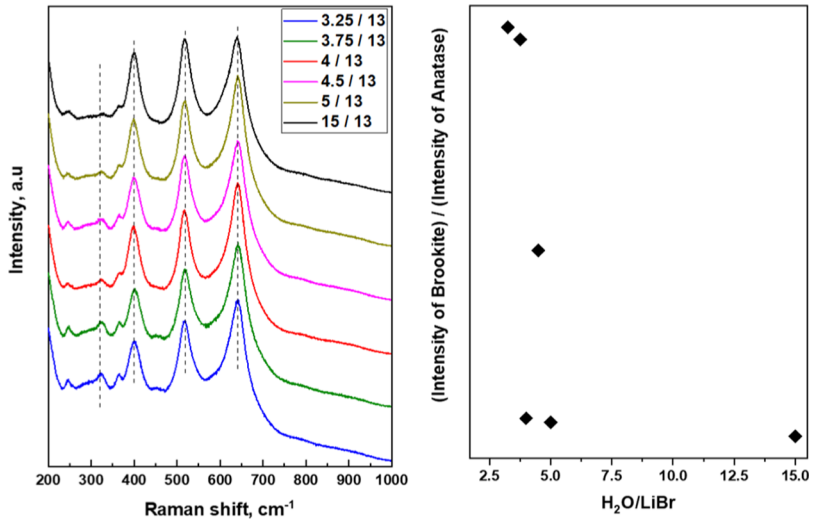

Figure 3. Ex situ Raman spectra of TiO_2 samples prepared at different H_2O/LiBr molar ratio (left) and change of the apparent brookite/anatase amount (right) as described by the intensity ratio of the 325 cm^{-1}(brookite) and 400 cm^{-1} (anatase) Raman bands.

opposed to 145 cm^{-1} for the post-calcined material. This is ascribed to the smaller size of crystallites that are formed during the synthesis and drying procedure.[41,42] It is known that sol−gel methods usually lead to amorphous or poorly crystalline TiO_2 materials.[24,43,44] This arises from the fact that the rates of hydrolysis and condensation are usually very fast and hard to control due to the presence of excess of water. We believe that the presence of crystalline domains in our samples, as the Raman data indicate, might be due to the minimal amount of water present in the reaction medium that allows the crystallization process of TiO_2 material to occur. In addition, the significant amount of ions, due to the dissociation of LiBr, may act as complexing agents, which in turn may also decrease either the hydrolysis or condensation rates. This hypothesis is in line with a modified sol−gel method reported elsewhere, where titanium alkoxides undergo hydrolysis/condensation in a controlled manner in the presence of 1 M NaCl and pluronic P-123 triblock copolymer.[45] It is evident that upon heating, the frequency as well as the width of the anatase peaks change significantly. Specifically, the $E_g(\nu_6)$ band at 150 cm^{-1} shifts to higher wavenumbers (155 cm^{-1}) and broadens. The bands at 399, 518, and 639 cm^{-1} broaden as well but shift to lower wavenumbers. This behavior is in agreement with reported temperature-dependent spectra of TiO_2 nanocrystals where phonon confinement, nonstoichiometric domains, as well as anharmonic effects have been proposed to contribute to this behavior.[40,42,46]

As our synthesis procedure leads to the incorporation of a small fraction of brookite in the TiO_2 anatase, one expects that the apparent blue shift observed on the $E_g(\nu_6)$ band will have a contribution from changes occurring in the brookite phase as well upon heating. Toward this, it is our intent to probe the sequential changes of the individual components that lead to the overall convoluted 150 cm^{-1} spectral shift. 2D-correlation Raman spectra have been constructed by using the dynamic Raman data acquired at different temperatures and an average spectrum as the reference. The synchronous and asynchronous spectra are shown in Figure 2a,b respectively. In general, the appearance of an autopeak (peak at the diagonal of the synchronous spectrum) suggests significant spectral intensity variations at the observed Raman shift.[47−50] The peaks located at the diagonal of the synchronous spectrum show the overall intensity susceptibility of two different spectral bands located at ∼148 and 160 cm^{-1} to the external perturbation that is applied,[49] which in our case is temperature. We ascribe these peaks to anatase and brookite bands, respectively. The presence of a negative sign of the cross peaks (peaks off diagonal that show a correlation between the two crystalline phases) implies that one of the Raman intensities (either of anatase or brookite) is increasing, while the other is decreasing.[48,49] In addition, the asynchronous spectrum

DOI: 10.1021/acsomega.9b02850
ACS Omega 2019, 4, 21302−21310

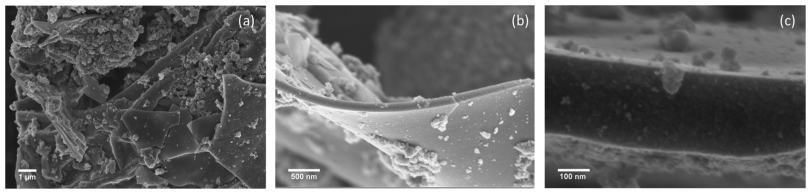

Figure 4. High-resolution SEM micrographs of the TiO_2 prepared at a H_2O/LiBr ratio equal to 3.75 at different level of magnification. Scale bars at (a) 1 μm, (b) 100 nm, and (c) 20 nm

(Figure 2b) shows two distinct cross peaks. As the sign of the synchronous and asynchronous cross peaks at the same spectral location (160, 145 cm^{-1}) is different, one can assume that changes in the brookite phase (spectral variation at 160 cm^{-1}) occur at a later stage than anatase (spectral variation at 145 cm^{-1}). Because temperature is monotonically increasing with time, we can assume that changes in the brookite phase start occurring at relatively higher temperatures (above 400 °C). In order to strengthen this argument, we have collected in situ Raman temperature-dependent spectra of commercial highly crystalline anatase for comparison and 2D Raman correlation has been also constructed (see Figure S3 of the Supporting Information). In the asynchronous spectrum, there is a pair of cross peaks at (145, 148 cm^{-1}) with a "butterfly" pattern that, according to Noda,[51] is indicative of a shift to higher wavenumbers highlighting that the aforementioned behavior is due to the presence of both anatase and brookite.

3.2. Effect of H_2O/LiBr on the Crystal Structure and Morphology of the Synthesized TiO_2. A systematic variation of the H_2O/LiBr ratio has been conducted in an effort to investigate possible changes in the crystalline phase, morphology, and physicochemical properties of the prepared TiO_2 materials. We have synthesized materials within the 3.25−5 range of the H_2O/LiBr ratio that is in line with the MSH regime. The Raman data shown in Figure 3a show that the dominant crystalline phase in all cases is anatase. However, a closer look of the Raman spectra reveals a monotonic trend that is also depicted in Figure 3b, that is, the higher the H_2O/LiBr ratio, the smaller the fraction of brookite observed. Exceeding the MSH regime (H_2O/LiBr equals to 15), brookite was observed at very low content. This observation could be explained by the fact that the addition of significant amount of salts in water leads to a pH decrease which in turn could favor the formation of mixed phases (anatase, brookite, rutile).[24] However, in our case, we do not observe any fraction of rutile crystal TiO_2. On the other hand, one cannot exclude the possibility of lattice matching between salt hydrates and TiO_2 crystal phases. $LiBr_x{\cdot}3H_2O$, that is very close to the H_2O/LiBr ratio of 3.25, as well as brookite, both have an orthorhombic structure, and thus, we hypothesize that small brookite domains might arise due to this lattice matching.[52] This is in agreement with recent research showing that lattice matching between salt solid crystals and the desired growing metal oxide is pivotal in controlling the crystal phase and overall morphology.[37] In the same work, the salt/precursor ratio is an important parameter that can potentially control the thickness of the final 2D-like oxide. We will discuss the effect of this ratio on our results in a later section.

To investigate the morphology of the synthesized TiO_2, SEM measurements were conducted on a series of materials that span the 3.25−5 range of the H_2O/LiBr ratio. In all materials, the LiBr/TTIP ratio has been kept constant at the value of 13. Micrographs of all MSH-derived TiO_2 are shown in the Supporting Information (Figure S4). All TiO_2 samples that have been prepared using molten LiBr hydrates at different ratios as reaction media show the presence of flakes or even thin, film-like materials of various sizes, shapes, and thickness. In the presence of H_2O/LiBr = 3.25, we observe thick flakes with irregular shapes and sizes within ∼0.5−4 μm. Increasing H_2O/LiBr, the apparent lateral size of the flakes increases, whereas the thickness seems to slightly decrease. These results highlight the possibility of controlling the size and thickness of the prepared TiO_2 flakes by adjusting the amount of water present in the MSH medium. At higher H_2O/LiBr but still within the MSH regime, in addition to very small TiO_2 flakes, larger sheets of ∼20 μm were also observed.

High-resolution SEM images were collected to further investigate the morphological behavior of the synthesized TiO_2 flakes. In Figure 4a−c we show the high-resolution micrographs of the TiO_2 prepared at a H_2O/LiBr ratio equal to 3.75 as a representative material with flakes of relatively large aspect ratio. Low magnification of the materials recovered through this synthesis protocol shows aggregates of ∼20−30 μm comprising many flakes. A closer look reveals that the TiO_2 flakes coexist with very small particles with an apparent spherical geometry. Higher magnification of the TiO_2 flakes show a thickness in the range of 50−150 nm. Focusing at the edge of the TiO_2 flakes, one can clearly observe that these flakes are composed via ordered agglomeration of spherical nanoparticles within the 5−10 nm range.

In order to elucidate structural differences between the different prepared samples, we studied the morphology of representative samples via TEM. Representative TEM images are shown in Figure 5 for the sample with H_2O/LiBr at 3.25 at different levels of magnification. In the images shown, at low magnification, we observe thin film-like agglomerates of various sizes with a large aspect ratio. At low H_2O/LiBr ratio, the TiO_2 films appear to be smaller in the lateral direction and thicker that those prepared at higher H_2O/LiBr (see the Supporting Information). HRTEM images reveal that small crystalline TiO_2 nanoparticles with an average particle size within 5−7 nm are assembled in such a way that an apparent 2D-like growth is achieved (Figure S5). We also observe the coexistence of anatase and brookite crystalline phases of TiO_2, as shown in the fast Fourier transform image where both anatase (101) and brookite (211) facets can be visualized. This result is in agreement with our Raman and XRD results discussed earlier. From the TEM images presented herein, it is also shown that the agglomeration of the nanoparticles to thin TiO_2 flakes leads to interparticle free space in the mesoporous regime. This result, in conjunction with the very small particle size observed in most of the samples, is indicative of a potential high surface area. To investigate this more, we conducted surface area and porosity measurements that are discussed next.

DOI: 10.1021/acsomega.9b02850
ACS Omega 2019, 4, 21302−21310

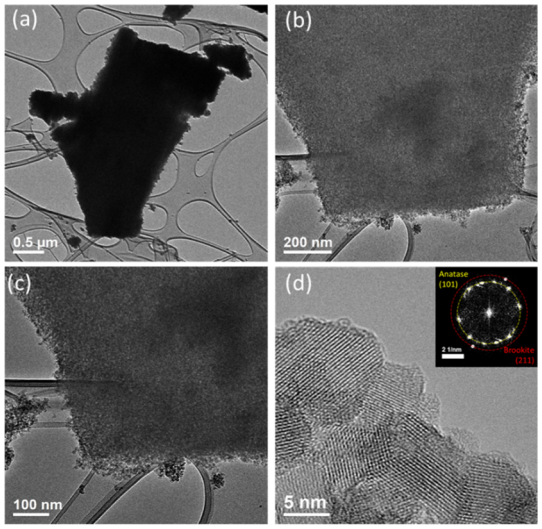

Figure 5. TEM images of the synthesized TiO_2 flakes at H_2O/LiBr molar ratio equal to 3.25 and LiBr/TTIP equal to 13. The material shown here has been calcined at 400 °C with 2 °C/min rate.

BET surface area along with porosity measurements were conducted for all synthesized samples and are summarized in Table 1. We find that the TiO_2 samples prepared show surface area ~200 m^2/g with the highest pore volume to be around 0.27 cm^3/g for the sample 3.25/13. The surface area seems to be constant throughout the different synthesized samples that were prepared within the MSH regime; outside this regime (sample 15/13), the surface area decreases. The relatively high surface area arises from the very small size of the TiO_2 nanoparticles, but one cannot exclude always the possibility of a contribution due to small amorphous domains. The adsorption isotherms and pore-size distribution of all samples are presented in Figure 6a,b. For some samples, we observe an H2 type of hysteresis loop, which is indicative of possible pore blocking and/or cavitation-induced evaporation.[53] The presented results herein show mesoporous materials with pore sizes in the range of 4−8 nm. We ascribe this "well-defined" behavior to the ordered agglomeration of the TiO_2 nanoparticles, as we discussed earlier in our TEM results. We believe that this ordered agglomeration allows the nanoparticles to rearrange and reorganize themselves in a unique way, thus creating interparticle space with similar size (apparent mesopore diameter).

Table 1. Specific Surface Area and Pore Volume of the Synthesized TiO_2 Materials at Different H_2O/LiBr Molar Ratio

samples (H_2O/LiBr)/(LiBr/TTIP)	BET surface area (m^2/g)	pore volume (cm^3/g)
3.25/13	201	0.266
3.75/13	208	0.238
4/13	198	0.192
4.5/13	205	0.201
5/13	199	0.184
15/13	172	0.131

3.3. Effect of LiBr/TTIP on the Purity and Thickness of TiO_2 Flakes. To further examine pertinent morphological and structural changes, the ratio between the salt added in water and the required metal oxide precursor, that is, the LiBr/TTIP ratio, is studied in this section. We hypothesize that lower amounts of TiO_2 precursor can lead to thinner TiO_2 films while maintaining similar morphology, as described in the previous section. In Figure 7, we report the Raman spectra of four samples, at different (13, 50, 80, and 120) LiBr/TTIP and same (3.75) H_2O/LiBr ratio. In all four samples, the anatase crystalline form of TiO_2 is maintained and is the dominant phase. A closer look reveals that by increasing the LiBr/TTIP ratio, our synthesis methods lead to a higher intensity of the anatase vibrational bands, indicating more uniform and overall pure TiO_2-anatase material. In addition, at high LiBr/TTIP ratio, the vibrational bands are sharper, underscoring much higher crystallinity of the synthesized samples. It is worth mentioning here that the bands pertaining to brookite decrease significantly as we increase the LiBr/TTIP ratio, thus highlighting the possibility of controlling the relative concentration between the two different crystalline phases. Similar spectral trend was found for other samples that were prepared, and pertinent Raman spectra are shown in the Supporting Information (Figure S5). The relative brookite/anatase ratio is also shown in Figure 7. The statistical significance of the synthesized materials at a low LiBr/TTIP ratio is larger than the error at high LiBr/TTIP. It is worth

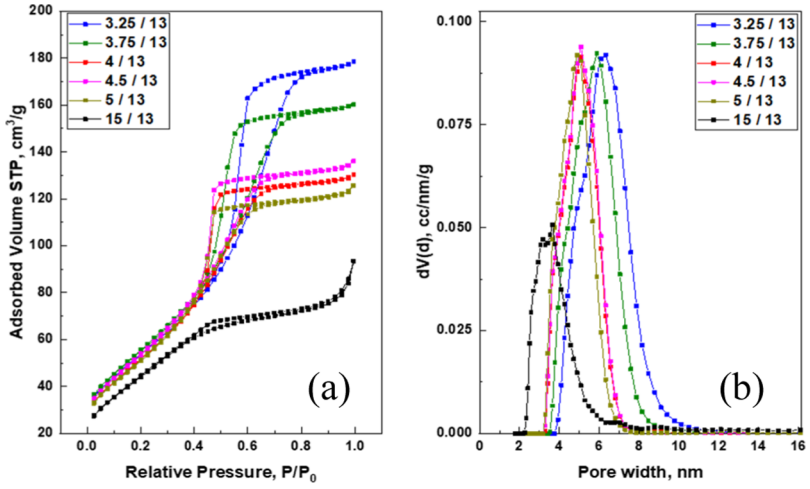

Figure 6. (a) N_2 physisorption isotherms and (b) pore-size distribution.

DOI: 10.1021/acsomega.9b02850
ACS Omega 2019, 4, 21302−21310

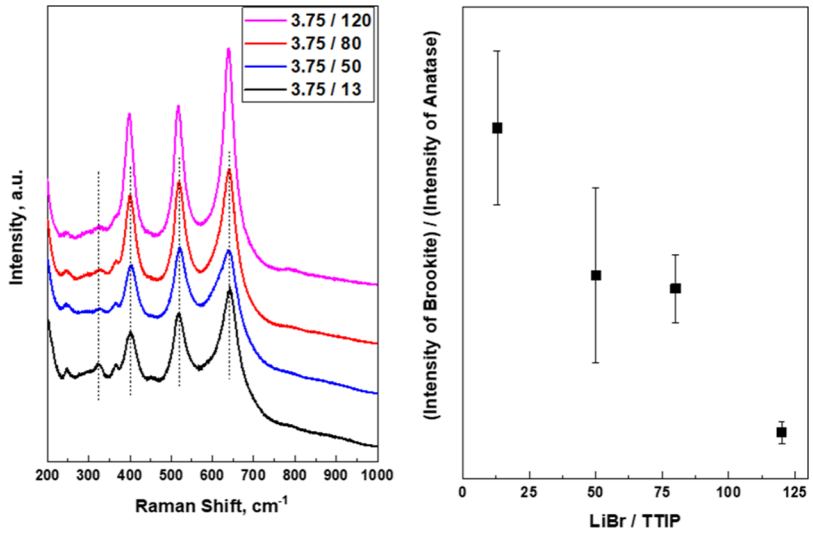

Figure 7. Ex -situ Raman spectra of TiO_2 samples prepared at same H_2O/LiBr molar ratio equal to 3.75 and different LiBr/TTIP molar ratios. The apparent brookite/anatase amount as described by the intensity ratio of relevant Raman bands is also depicted.

highlighting here that we use Raman spectroscopy where the incident beam is directed on the surface through a microscope objective. Depending on the sample location as well as the spatial resolution of the objective, the spectra for the same material might slightly differ due to the different contribution of larger or smaller crystallites to the overall spectrum. To estimate the reported statistical error (Figure 7), two different objectives (10× and 100×) have been used and five measurements at different locations have been averaged. Relevant data are shown in the Supporting Information (Figure S6). The TEM images for samples that have been synthesized at H_2O/LiBr ratio 3.25 and high LiBr/TTIP ratio (50) are shown in Figure 8. The results support our hypothesis

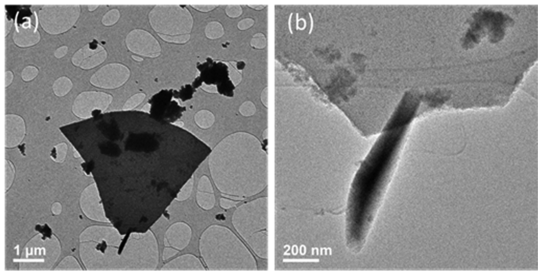

Figure 8. TEM images of the synthesized TiO_2 flakes at H_2O/LiBr molar ratio equal to 3.25 and LiBr/TTIP equal to 50. The material shown here has been calcined at 400 °C.

that lower amounts of the precursor lead to thinner TiO_2 films, whereas the lateral size seems to also decrease. Similar nanoparticle agglomeration was also observed under these synthesis conditions. These results underscore the possibility of controlling the apparent thickness of the synthesized TiO_2 flakes by carefully tuning the synthesis parameters. Future work on parametrization and optimization of our synthesis method can shed light in this direction.

3.4. Insights into the Nature of the Synthesis Route and Potential Scalability. This work focuses on the use of MSHs and specifically LiBr hydrates as non-trivial synthesis solvent media. As mentioned earlier, these solutions have water to salt molar ratio equal or less than the coordination number of the cation. It is reported that MSHs can be described as low-temperature melts that exhibit only ion−water interactions, with no water−water or ion−ion interactions taking place. In addition to the fact that the ions of the salt are not well separated, these solutions have the ability to maintain an ordered structure of water within the salt ions.[52] We hypothesize that this ordered structure is responsible for the ordered agglomeration of small TiO_2 nanoparticles in an apparent film-like morphology. As the titanium alkoxide precursor reacts very fast with water molecules, we believe that the hydrolysis and condensation occur rapidly in the regimes of water molecules that interact only with the dissociated ions. Because of minimal water−water interactions within the solvent system, we also hypothesize that further TiO_2 condensation in the directions that can lead to bulk agglomerates is prohibited.

In addition, the MSH solvent media show low water activity,[54] high acidity (especially in the presence of acids[38]), and enhanced viscosity.[55] All these parameters could be potentially critical in the synthesis of metal oxides. For instance, it has been reported that the change in the viscosity of the synthesis medium can have a significant effect on the formation of thin TiO_2 flakes.[56] As there is an increased viscosity of the MSH medium as compared to neat water, the possibility that this slightly affects the morphology of the flakes cannot be excluded. However, by changing the stirring speed in our synthesis procedure, we do not observe significant change in the thickness or the apparent "aspect ratio" of the synthesized flakes and thus we hypothesize that viscosity might have a minimal effect. In future work, we aim to parametrize and optimize our procedure in order to establish an overall synthetic protocol that leads to predictable morphologies. Via this optimization, we anticipate providing in the future, molecular-level understanding as well as detailed mechanistic insights into the actual synthesis steps.

Finally, it is worth mentioning here that a rather important, not trivial, benefit of the use of concentrated LiBr is highly related with the scalability potential of the presented synthesis. The hydrolysis of the precursors, that is, TTIP, leads to the release of significant amount of isopropanol (IPA) that needs to be separated from the aqueous mixture. However, the strong azeotrope between IPA and H_2O could potentially hamper any

DOI: 10.1021/acsomega.9b02850
ACS Omega 2019, 4, 21302−21310

attempt for scaling up and reusability of both solvent(s) and salt system. The use of concentrated LiBr has been reported to break the azeotrope and thus more than 99% IPA recovery can be achieved,[57] highlighting the possibility of utilizing the MSH systems in reasonably scaled-up processes. To that extent, future technoeconomic analysis of the synthesis process will be beneficial in order to develop a holistic synthesis protocol at a scaled-up level.

4. CONCLUSIONS

The manufacturing of TiO_2 from titanium-containing ores relies mainly on the sulfate and chloride processes which are energy intensive as well as not environmentally friendly because they generate large amount of acidic waste. Thus, the search for new, facile, and scalable synthesis approaches to produce TiO_2 is always of topical character. The aspect of scalability becomes even more challenging if one takes into account the need of tuning the morphology and crystalline structure of TiO_2, which in turn can control the overall physicochemical properties of the synthesized material. In this article, we present a method for the synthesis of titanium dioxide with a high surface area and apparent mesoporous structure. The large surface area arises from the small size of the TiO_2 nanoparticles present in the larger aggregates, whereas the apparent mesoporosity is from the intercrystalline space between those nanoparticles. The synthesized materials present good thermal stability up to 400 °C. More specifically, the TiO_2 material prepared by using MSHs, such as molten LiBr hydrate solution, as reaction media show a thin, flake-like morphology with a relatively large aspect ratio. We find that the thickness of the prepared flakes depends primarily on the LiBr/water molar ratio (always within the MSH regime). In all cases, the primary crystalline phase of TiO_2 is anatase but small fraction of brookite has been also observed. In this work, it is shown that the amount of brookite formed depends on both $LiBr/H_2O$ as well as LiBr/precursor molar ratio. We hypothesize that the flake-like morphology arises from the fact that fast hydrolysis and condensation takes place within the ordered structure of water molecules in the MSH system.

■ ASSOCIATED CONTENT

Supporting Information

The Supporting Information is available free of charge at https://pubs.acs.org/doi/10.1021/acsomega.9b02850.

Detailed XRD patterns, FESEM images, TEM images, Raman spectra, and 2D Raman maps (PDF)

■ AUTHOR INFORMATION

Corresponding Author

*E-mail: g.tsilo@rutgers.edu.

ORCID

George Tsilomelekis: 0000-0002-0435-8216

Notes

The authors declare no competing financial interest.

■ ACKNOWLEDGMENTS

This material is based upon work supported in part by Rutgers, The State University of New Jersey, and the National Science Foundation Award #1751683. The TEM analysis conducted by W.Z. was financially supported by the Catalysis Center for Energy Innovation, an Energy Frontier Research Center funded by the U.S. Department of Energy, Office of Science, Office of Basic Energy Sciences under award number DESC0001004. The authors would like to thank Prof. Alexander Neimark for helping with the BET measurements and porosity analysis.

■ ABBREVIATIONS

MSS, molten salt synthesis; MSH, molten salt hydrates

■ REFERENCES

(1) Nisar, J.; Topalian, Z.; De Sarkar, A.; Österlund, L.; Ahuja, R. TiO2-Based Gas Sensor: A Possible Application to SO2. *ACS Appl. Mater. Interfaces* **2013**, *5*, 8516−8522.

(2) Wang, Y.; Liu, L.; Meng, C.; Zhou, Y.; Gao, Z.; Li, X.; Cao, X.; Xu, L.; Zhu, W. A novel ethanol gas sensor based on TiO2/Ag0.35V2O5 branched nanoheterostructures. *Sci. Rep.* **2016**, *6*, 33092.

(3) Ruiz, A. M.; Sakai, G.; Cornet, A.; Shimanoe, K.; Morante, J. R.; Yamazoe, N. Cr-doped TiO2 gas sensor for exhaust NO2 monitoring. *Sens. Actuators, B* **2003**, *93*, 509−518.

(4) Wagemaker, M.; Borghols, W. J. H.; van Eck, E. R. H.; Kentgens, A. P. M.; Kearley, G. J.; Mulder, F. M. The Influence of Size on Phase Morphology and Li-Ion Mobility in Nanosized Lithiated Anatase TiO2. *Chem.—Eur. J.* **2007**, *13*, 2023−2028.

(5) He, Y. J.; Peng, J. F.; Chu, W.; Li, Y. Z.; Tong, D. G. Retracted Article: Black mesoporous anatase TiO2 nanoleaves: a high capacity and high rate anode for aqueous Al-ion batteries. *J. Mater. Chem. A* **2014**, *2*, 1721−1731.

(6) Xiong, H.; Slater, M. D.; Balasubramanian, M.; Johnson, C. S.; Rajh, T. Amorphous TiO2 Nanotube Anode for Rechargeable Sodium Ion Batteries. *J. Phys. Chem. Lett.* **2011**, *2*, 2560−2565.

(7) Ge, M.; Cao, C.; Huang, J.; Li, S.; Chen, Z.; Zhang, K.-Q.; Al-Deyab, S. S.; Lai, Y. A review of one-dimensional TiO2 nanostructured materials for environmental and energy applications. *J. Mater. Chem. A* **2016**, *4*, 6772−6801.

(8) Zhang, X.; Peng, T.; Song, S. Recent advances in dye-sensitized semiconductor systems for photocatalytic hydrogen production. *J. Mater. Chem. A* **2016**, *4*, 2365−2402.

(9) Zukalová, M.; Zukal, A.; Kavan, L.; Nazeeruddin, M. K.; Liska, P.; Grätzel, M. Organized Mesoporous TiO2 Films Exhibiting Greatly Enhanced Performance in Dye-Sensitized Solar Cells. *Nano Lett.* **2005**, *5*, 1789−1792.

(10) Zhang, W.; Zhu, R.; Ke, L.; Liu, X.; Liu, B.; Ramakrishna, S. Anatase Mesoporous TiO2 Nanofibers with High Surface Area for Solid-State Dye-Sensitized Solar Cells. *Small* **2010**, *6*, 2176−2182.

(11) Ge, M.; Cai, J.; Iocozzia, J.; Cao, C.; Huang, J.; Zhang, X.; Shen, J.; Wang, S.; Zhang, S.; Zhang, K.-Q.; Lai, Y.; Lin, Z. A review of TiO2 nanostructured catalysts for sustainable H2 generation. *Int. J. Hydrogen Energy* **2017**, *42*, 8418−8449.

(12) Garcia, A.; Yan, N.; Vincent, A.; Singh, A.; Hill, J. M.; Chuang, K. T.; Luo, J.-L. Highly cost-effective and sulfur/coking resistant VOx-grafted TiO2 nanoparticles as an efficient anode catalyst for direct conversion of dry sour methane in solid oxide fuel cells. *J. Mater. Chem. A* **2015**, *3*, 23973−23980.

(13) Fujishima, A.; Honda, K. Electrochemical Photolysis of Water at a Semiconductor Electrode. *Nature* **1972**, *238*, 37−38.

(14) Green, I. X.; Tang, W.; Neurock, M.; Yates, J. T. Spectroscopic Observation of Dual Catalytic Sites During Oxidation of CO on a Au/TiO_2 Catalyst. *Science* **2011**, *333*, 736.

(15) Shi, Q.; Li, Y.; Zhou, Y.; Miao, S.; Ta, N.; Zhan, E.; Liu, J.; Shen, W. The shape effect of TiO2 in VOx/TiO2 catalysts for selective reduction of NO by NH3. *J. Mater. Chem. A* **2015**, *3*, 14409−14415.

(16) Dzwigaj, S.; Louis, C.; Breysse, M.; Cattenot, M.; Bellière, V.; Geantet, C.; Vrinat, M.; Blanchard, P.; Payen, E.; Inoue, S.; Kudo, H.; Yoshimura, Y. New generation of titanium dioxide support for hydrodesulfurization. *Appl. Catal., B* **2003**, *41*, 181−191.

DOI: 10.1021/acsomega.9b02850
ACS Omega 2019, 4, 21302−21310

(17) Panagiotopoulou, P.; Christodoulakis, A.; Kondarides, D. I.; Boghosian, S. Particle size effects on the reducibility of titanium dioxide and its relation to the water−gas shift activity of Pt/TiO2 catalysts. *J. Catal.* **2006**, *240*, 114−125.
(18) Grabowski, R.; Grzybowska, B.; Samson, K.; Słoczyński, J.; Stoch, J.; Wcisło, K. Effect of alkaline promoters on catalytic activity of V2O5/TiO2 and MoO3/TiO2 catalysts in oxidative dehydrogenation of propane and in isopropanol decomposition. *Appl. Catal., A* **1995**, *125*, 129−144.
(19) Tsilomelekis, G.; Boghosian, S. On the configuration, molecular structure and vibrational properties of MoOx sites on alumina, zirconia, titania and silica. *Catal. Sci. Technol.* **2013**, *3*, 1869−1888.
(20) Tsilomelekis, G.; Boghosian, S. An operando Raman study of molecular structure and reactivity of molybdenum(vi) oxide supported on anatase for the oxidative dehydrogenation of ethane. *Phys. Chem. Chem. Phys.* **2012**, *14*, 2216−2228.
(21) Ma, Y.; Li, Y.; Mao, M.; Hou, J.; Zeng, M.; Zhao, X. Synergetic effect between photocatalysis on TiO2 and solar light-driven thermocatalysis on MnOx for benzene purification on MnOx/TiO2 nanocomposites. *J. Mater. Chem. A* **2015**, *3*, 5509−5516.
(22) Henderson, M. A. A surface science perspective on TiO2 photocatalysis. *Surf. Sci. Rep.* **2011**, *66*, 185−297.
(23) Nakata, K.; Fujishima, A. TiO2 photocatalysis: Design and applications. *J. Photochem. Photobiol., C* **2012**, *13*, 169−189.
(24) Cargnello, M.; Gordon, T. R.; Murray, C. B. Solution-phase synthesis of titanium dioxide nanoparticles and nanocrystals. *Chem. Rev.* **2014**, *114*, 9319−9345.
(25) Zywitzki, D.; Jing, H.; Tüysüz, H.; Chan, C. K. High surface area, amorphous titania with reactive Ti3+ through a photo-assisted synthesis method for photocatalytic H2 generation. *J. Mater. Chem. A* **2017**, *5*, 10957−10967.
(26) Soler-Illia, G. J. A. A.; Angelomé, P. C.; Fuertes, M. C.; Grosso, D.; Boissiere, C. Critical aspects in the production of periodically ordered mesoporous titania thin films. *Nanoscale* **2012**, *4*, 2549−2566.
(27) Nakata, K.; Fujishima, A. TiO2 photocatalysis: Design and applications. *J. Photochem. Photobiol., C* **2012**, *13*, 169−189.
(28) Wang, T.; Liu, L.; Ge, G.; Liu, M.; Zhou, W.; Chang, K.; Yang, F.; Wang, D.; Ye, J. Two-dimensional titanium oxide nanosheets rich in titanium vacancies as an efficient cocatalyst for photocatalytic water oxidation. *J. Catal.* **2018**, *367*, 296−305.
(29) Feng, J.; Yin, M.; Wang, Z.; Yan, S.; Wan, L.; Li, Z.; Zou, Z. Facile synthesis of anatase TiO2 mesocrystal sheets with dominant {001} facets based on topochemical conversion. *CrystEngComm* **2010**, *12*, 3425.
(30) Liu, G.; Yang, H. G.; Pan, J.; Yang, Y. Q.; Lu, G. Q.; Cheng, H.-M. Titanium dioxide crystals with tailored facets. *Chem. Rev.* **2014**, *114*, 9559−9612.
(31) Leng, M.; Chen, Y.; Xue, J. Synthesis of TiO2 nanosheets via an exfoliation route assisted by a surfactant. *Nanoscale* **2014**, *6*, 8531−8534.
(32) Roy, B.; Ahrenkiel, S. P.; Fuierer, P. A. Controlling the Size and Morphology of TiO2Powder by Molten and Solid Salt Synthesis. *J. Am. Ceram. Soc.* **2008**, *91*, 2455−2463.
(33) Reddy, M. V.; Adams, S.; Liang, G. T. J.; Mingze, I. F.; Van Tu An, H.; Chowdari, B. V. R. Low temperature molten salt synthesis of anatase TiO2 and its electrochemical properties. *Solid State Ionics* **2014**, *262*, 120−123.
(34) Peining, Z.; Yongzhi, W.; Reddy, M. V.; Sreekumaran Nair, A.; Shengjie, P.; Sharma, N.; Peterson, V. K.; Chowdari, B. V. R.; Ramakrishna, S. TiO2 nanoparticles synthesized by the molten salt method as a dual functional material for dye-sensitized solar cells. *RSC Adv.* **2012**, *2*, 5123.
(35) Hu, Z.; Xiao, X.; Jin, H.; Li, T.; Chen, M.; Liang, Z.; Guo, Z.; Li, J.; Wan, J.; Huang, L.; Zhang, Y.; Feng, G.; Zhou, J. Rapid mass production of two-dimensional metal oxides and hydroxides via the molten salts method. *Nat. Commun.* **2017**, *8*, 15630.
(36) Susman, M. D.; Pham, H. N.; Datye, A. K.; Chinta, S.; Rimer, J. D. Factors Governing MgO(111) Faceting in the Thermal Decomposition of Oxide Precursors. *Chem. Mater.* **2018**, *30*, 2641−2650.
(37) Xiao, X.; Song, H.; Lin, S.; Zhou, Y.; Zhan, X.; Hu, Z.; Zhang, Q.; Sun, J.; Yang, B.; Li, T.; Jiao, L.; Zhou, J.; Tang, J.; Gogotsi, Y. Scalable salt-templated synthesis of two-dimensional transition metal oxides. *Nat. Commun.* **2016**, *7*, 11296.
(38) Deng, W.; Kennedy, J. R.; Tsilomelekis, G.; Zheng, W.; Nikolakis, V. Cellulose Hydrolysis in Acidified LiBr Molten Salt Hydrate Media. *Ind. Eng. Chem. Res.* **2015**, *54*, 5226−5236.
(39) Voigt, W.; Zeng, D. Solid-liquid equilibria in mixtures of molten salt hydrates for the design of heat storage materials. *Pure Appl. Chem.* **2002**, *74*, 1909.
(40) Ohsaka, T. Temperature Dependence of the Raman Spectrum in Anatase TiO2. *J. Phys. Soc. Jpn.* **1980**, *48*, 1661−1668.
(41) Zhang, W. F.; He, Y. L.; Zhang, M. S.; Yin, Z.; Chen, Q. Raman scattering study on anatase TiO2nanocrystals. *J. Phys. D: Appl. Phys.* **2000**, *33*, 912−916.
(42) Zhang, J.; Li, M.; Feng, Z.; Chen, J.; Li, C. UV Raman Spectroscopic Study on TiO2. I. Phase Transformation at the Surface and in the Bulk. *J. Phys. Chem. B* **2006**, *110*, 927−935.
(43) Fattakhova-Rohlfing, D.; Zaleska, A.; Bein, T. Three-dimensional titanium dioxide nanomaterials. *Chem. Rev.* **2014**, *114*, 9487−9558.
(44) Simonsen, M. E.; Søgaard, E. G. Sol-gel reactions of titanium alkoxides and water: influence of pH and alkoxy group on cluster formation and properties of the resulting products. *J. Sol-Gel Sci. Technol.* **2010**, *53*, 485−497.
(45) Han, S.; Choi, S.-H.; Kim, S.-S.; Cho, M.; Jang, B.; Kim, D.-Y.; Yoon, J.; Hyeon, T. Low-temperature synthesis of highly crystalline TiO2 nanocrystals and their application to photocatalysis. *Small* **2005**, *1*, 812−816.
(46) Scepanovic, M.; Grujic-Brojcin, M.; Dohcevic-Mitrovic, Z. D.; Popovic, Z. V. Characterization of anatase TiO2 nanopowder by variable-temperature Raman spectroscopy. *Sci. Sintering* **2009**, *41*, 67−73.
(47) Lasch, P.; Noda, I. Two-Dimensional Correlation Spectroscopy (2D-COS) for Analysis of Spatially Resolved Vibrational Spectra. *Appl. Spectrosc.* **2019**, *73*, 359−379.
(48) Noda, I. Two-Dimensional Infrared (2D IR) Spectroscopy: Theory and Applications. *Appl. Spectrosc.* **1990**, *44*, 550−561.
(49) Noda, I. Generalized Two-Dimensional Correlation Method Applicable to Infrared, Raman, and Other Types of Spectroscopy. *Appl. Spectrosc.* **1993**, *47*, 1329−1336.
(50) Mee Jung, Y.; Noda, I. New Approaches to Generalized Two-Dimensional Correlation Spectroscopy and Its Applications. *Appl. Spectrosc. Rev.* **2006**, *41*, 515−547.
(51) Noda, I.; Ozaki, Y. *Two-Dimensional Correlation Spectroscopy: Applications in Vibrational and Optical Spectroscopy*; John Wiley & Sons, Ltd, 2005.
(52) Sohr, J.; Schmidt, H.; Voigt, W. Higher hydrates of lithium chloride, lithium bromide and lithium iodide. *Acta Crystallogr., Sect. C: Struct. Chem.* **2018**, *74*, 194−202.
(53) Thommes, M.; Kaneko, K.; Neimark, A. V.; Olivier, J. P.; Rodriguez-Reinoso, F.; Rouquerol, J.; Sing, K. S. W. Physisorption of gases, with special reference to the evaluation of surface area and pore size distribution (IUPAC Technical Report). *Pure Appl. Chem.* **2015**, *87*, 1051−1069.
(54) Zeng, D.; Voigt, W. Phase diagram calculation of molten salt hydrates using the modified BET equation. *Calphad* **2003**, *27*, 243−251.
(55) Minevich, A.; Marcus, Y.; Ben-Dor, L. Densities of Solid and Molten Salt Hydrates and Their Mixtures and Viscosities of the Molten Salts. *J. Chem. Eng. Data* **2004**, *49*, 1451−1455.
(56) Yang, M.-C.; Lee, Y.-Y.; Xu, B.; Powers, K.; Meng, Y. S. TiO2 flakes as anode materials for Li-ion-batteries. *J. Power Sources* **2012**, *207*, 166−172.
(57) Vora, S. R.; Thakore, S. B.; Padhiyar, N.; Pathan, A. Effect Of Addition Of LiBr Salt In Iso-Propanol - Water Binary Azeotropic Mixture. *Int. J. Sci. Eng. Technol.* **2013**, *2*, 245−248.

DOI: 10.1021/acsomega.9b02850
ACS Omega 2019, 4, 21302−21310